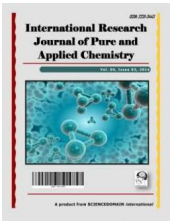

International Research Journal of Pure & Applied Chemistry
11(1): 1-10, 2016, Article no.IRJPAC.23674
ISSN: 2231-3443, NLM ID: 101647669

SCIENCEDOMAIN *international*
www.sciencedomain.org

Crystal Structure and Thermal Properties of $SrC_4H_4O_6 \cdot 4H_2O$ Single Crystals

T. Fukami[1*], S. Tahara[1], C. Yasuda[1] and K. Nakasone[1]

[1]Department of Physics and Earth Sciences, Faculty of Science, University of the Ryukyus, Okinawa 903-0213, Japan.

Authors' contributions

This work was carried out in collaboration between all authors. Author TF performed experiments, managed the literature searches and wrote the first draft of the manuscript. Authors ST, CY and KN revised the manuscript and participated in group discussions. All authors read and approved the final manuscript.

Article Information

DOI: 10.9734/IRJPAC/2016/23674
Editor(s):
(1) Wolfgang Linert, Institute of Applied Synthetic Chemistry Vienna University of Technology Getreidemarkt, Austria.
Reviewers:
(1) Ravi Kant, Maharaja Ranjit Singh Sate Technical University, Bathinda, India.
(2) S. Natarajan, Madurai Kamaraj University, India.
Complete Peer review History: http://sciencedomain.org/review-history/13060

Original Research Article

Received 15th December 2015
Accepted 11th January 2016
Published 25th January 2016

ABSTRACT

Single crystals of strontium tartrate tetrahydrate, $SrC_4H_4O_6 \cdot 4H_2O$, were grown at 308 K by a gel method using silica gel as the medium of growth. Differential scanning calorimetry, thermogravimetric-differential thermal analysis, and X-ray diffraction measurements were performed on the single crystals. The space group symmetry (orthorhombic $P2_12_12_1$) and the structural parameters were determined at room temperature. The O–H–O hydrogen-bonded network formed between adjacent $C_4H_4O_6$ molecules was found to extend along the *a*-axis. Weight losses due to thermal decomposition of $SrC_4H_4O_6 \cdot 4H_2O$ occurred in the temperature range of 350–1200 K. The weight losses during decomposition were suggested to be caused by the evaporation of bound water molecules and the evolution of H_2CO, $1/2O_2$, and 2CO gases. The chalky white substance remaining in the open vessel after decomposition was strontium oxide, SrO.

Keywords: $SrC_4H_4O_6 \bullet 4H_2O$; crystal structure; thermal decomposition; DSC; TG-DTA; X-ray.

**Corresponding author: E-mail: fukami@sci.u-ryukyu.ac.jp;*

1. INTRODUCTION

The two types of tartrate salt are represented by two different chemical formulas, which have two monovalent cations or one bivalent cation: $MMC_4H_4O_6{\cdot}xH_2O$ (M^+ = H^+, Li^+, Na^+, K^+, Cs^+, or NH_4^+) and $BC_4H_4O_6{\cdot}xH_2O$ (B^{2+} = Ca^{2+}, Mn^{2+}, Fe^{2+}, Co^{2+}, Cu^{2+}, Zn^{2+}, Sr^{2+}, Sn^{2+}, Ba^{2+}, or Pb^{2+}), respectively [1-11]. Some of the compounds exhibit a range of interesting physical properties such as ferroelectricity, piezoelectricity, structural phase transitions and dielectric anomalies, and are used in ultrasonic transducers and microphones, as well as in linear and nonlinear mechanical devices [2,12-14]. More than 150 years ago, Louis Pasteur developed the first chiral separation of the enantiomers of sodium ammonium tartrate by utilizing the asymmetry of the crystals [15-17]. He found that a change in the optical rotation of plane-polarized light was induced by the different structures of the enantiomers in water solution. The discovery of enantiomers has played an important role in advancing the scientific understanding of molecular chirality.

Strontium tartrate ($SrC_4H_4O_6$) is known to have two different crystal structures. One is monoclinic with space group $P2_1$, and contains three independent water molecules in the structure. The positional and thermal parameters of the atoms in the crystal structure of $SrC_4H_4O_6{\cdot}3H_2O$ have been reported by Ambady [10]. The other is orthorhombic with space group $P2_12_12_1$, and contains four independent water molecules in the structure. The lattice parameters of $SrC_4H_4O_6{\cdot}4H_2O$ obtained from powder X-ray diffraction are close to those of calcium tartrate tetrahydrate, $CaC_4H_4O_6{\cdot}4H_2O$ [9,11]. However, the crystal structure of the $SrC_4H_4O_6{\cdot}4H_2O$ crystal has not yet been determined. The crystal structure of the strontium salt is expected to be close to that of the calcium salt. Moreover, a detailed description of the thermal properties of $SrC_4H_4O_6{\cdot}4H_2O$ has not yet been reported.

The purpose of this study is to determine the crystal structure of $SrC_4H_4O_6{\cdot}4H_2O$ at room temperature using X-ray diffraction measurements, and to obtain the thermal properties of the strontium salt using differential scanning calorimetry (DSC) and thermogravimetric-differential thermal analysis (TG-DTA) measurements.

2. EXPERIMENTAL

2.1 Crystal Growth

Single crystals of $SrC_4H_4O_6{\cdot}4H_2O$ were grown in silica gel medium at 308 K using the single test tube diffusion method. The gels were prepared in test tubes (length of 200 mm, and diameter of 30 mm) using solutions of 2M Na_2SiO_3 (20 ml), 1M $C_4H_6O_6$ (20 ml), and 2M CH_3COOH (20 ml), and aged for one day. A solution (20 ml) of 0.5 M $SrCl_2{\cdot}6H_2O$ was then gently poured on top of the gel. The crystals used were harvested after three months.

2.2 X-ray Crystal Structure Determination

The X-ray diffraction measurements were carried out using a Rigaku Saturn CCD X-ray diffractometer with graphite-monochromated Mo K_α radiation (λ = 0.71073 Å). The diffraction data were collected at 299 K using an ω scan mode with a crystal-to-detector distance of 40 mm, and processed using the CrystalClear software package. The sample used was spherical in shape with a diameter of 0.30 mm. The intensity data were corrected for Lorentz polarization and absorption effects. The structure was solved with direct methods using the SIR2011 program and refined on F^2 by full-matrix least-squares methods using the SHELXL-2013 program in the WinGX package [18-20].

2.3 Thermal Measurements

DSC and TG-DTA measurements were respectively carried out in the temperature ranges of 105–450 K and 300–1250 K, using DSC7020 and TG-DTA7300 systems from Seiko Instruments Inc. Aluminium (for DSC) and alumina (for TG-DTA) open pans with no pan cover were used as the measuring vessels and reference pans. Fine powder samples prepared from crushed single crystals were used for the measurements. The sample amount varied between 2.88 and 3.94 mg, and the heating rates were 5 or 10 K min^{-1} under a dry nitrogen gas flow.

3. RESULTS AND DISCUSSION

3.1 Crystal Structure

The crystal structure of $SrC_4H_4O_6{\cdot}4H_2O$ was determined at room temperature by X-ray diffraction. The lattice parameters calculated from all observed reflections showed that the

crystal belongs to an orthorhombic system. The intensity statistics and systematic extinctions in the observed reflections strongly indicated that the crystal belongs to an acentric point group, and the possible space group is $P2_12_12_1$. Thus, the space group of $SrC_4H_4O_6{\cdot}4H_2O$ was determined to be orthorhombic $P2_12_12_1$ with a = 9.4694(4) Å, b = 9.5130(3) Å, and c = 10.9703(3) Å. The atomic coordinates and thermal parameters for $SrC_4H_4O_6{\cdot}4H_2O$, including the positions of all hydrogen atoms, were determined at room temperature. A final R-factor of 4.01% was calculated for 5076 unique observed reflections. The relevant crystal data, as well as a summary of the intensity data collection and structure refinement parameters, are given in Table 1. Fig. 1 shows a perspective view of the crystal structure of $SrC_4H_4O_6{\cdot}4H_2O$. The positional parameters in fractions of a unit cell, and the thermal parameters are listed in Table 2. Selected bond lengths (in Å) and angles (in degrees) are given in Table 3. The hydrogen-bond geometry (in Å and degrees) is presented in Table 4.

The observed lattice parameters along the a- and c-axes are slightly larger than those of $CaC_4H_4O_6{\cdot}4H_2O$, whereas the parameter along the b-axis is slightly larger than that determined by the powder X-ray diffraction method for $SrC_4H_4O_6{\cdot}4H_2O$ [7-9,11]. The observed structure of the strontium salt contains four crystallographically independent H_2O molecules, and is very close to that of the calcium salt [7,8]. The fundamental features of the obtained structure are as follows. Each Sr atom in the unit cell is surrounded by eight O atoms at distances from 2.527(2) to 2.676(2) Å to form a SrO_8 dodecahedron, as shown in Table 3. The average Sr–O distance is 2.594 Å. The lengths of the six O–C bonds in a $C_4H_4O_6$ molecule are in the range of 1.241(4)–1.428(4) Å, as shown in Table 3. The variation in O–C distances is probably related to differences in bond type. The lengths of single and double O–C bonds in organic molecules are around 1.43 and 1.22 Å, respectively. The lengths of O(3)–C(2) and O(4)–C(3) bonds on hydroxyl group are about 1.43 Å. Thus, two of the O-C bonds have single bond character. As the lengths of the remaining four O–C bonds are about 1.25 Å, these bonds have double bond character. Moreover, the lengths of the three C–C bonds are in the range of 1.518(4)–1.541(4) Å. Because the length of a single C–C bond in organic molecules is around 1.54 Å, these three bonds have single bond character. Rotational symmetry of the $C_4H_4O_6$ molecule is seen about the axis perpendicular to

Table 1. Crystal data, intensity collection and structure refinement for $SrC_4H_4O_6{\cdot}4H_2O$ at room temperature

Compound, M_r	$SrC_4H_{12}O_{10}$, 307.75
Crystal shape, colour	Prism, yellowish
Crystal system, space group	Orthorhombic, $P2_12_12_1$
Lattice constants	a = 9.4694(4) Å, b = 9.5130(3) Å
	c = 10.9703(3) Å
V, Z	988.23(6), 4
D(cal.), μ(Mo K_α), F(000)	2.069 Mg m^{-3}, 5.496 mm^{-1}, 616
Sample shape, size in diameter	Sphere, 2r = 0.30 mm
θ range for data collection	2.83–38.07º
Index ranges	$-16 \le h \le 16$, $-16 \le k \le 16$, $-18 \le l \le 18$
Reflections collected, unique	28662, 5239 [R(int)=0.0458]
Completeness to θ_{max}	97.9%
Absorption correction type	Spherical
Transmission factor T_{min}–T_{max}	0.3176–0.3440
Date, parameter	5076 [$I>2\sigma(I)$], 185
Final R indices	R_1 = 0.0401, wR_2 = 0.0699
R indices (all data)	R_1 = 0.0428, wR_2 = 0.0713
Weighting scheme	$w = 1/[\sigma^2(F_o^2)+(0.0164P)^2+0.9939P]$
	$P = (F_o^2+2F_c^2)/3$
Goodness-of-fit on F^2	1.113
Extinction coefficient	0.019(1)
Largest diff. peak and hole	0.75 and -1.18 e Å^{-3}
Flack parameter	-0.013(3)

the C(2)–C(3) bond. In fact, the O(1)–C(1), O(2)–C(1), and O(3)–C(2) bond lengths, and O(1)–C(1)–O(2) angle are almost the same as the O(5)–C(4), O(6)–C(4), and O(4)–C(3) bond lengths, and O(5)–C(4)–O(6) angle, respectively, as shown in Table 3. The angle between the two least-squares planes of atoms, O(1)O(2)O(3)C(1)C(2) and O(4)O(5)O(6)C(3)C(4), in the $C_4H_4O_6$ molecule is 88.7(1)º, which is close to a right angle (90º). These bond lengths and angles for $C_4H_4O_6$ in the $SrC_4H_4O_6{\cdot}4H_2O$ structure are very close to those observed in $CaC_4H_4O_6{\cdot}4H_2O$ [7,8].

Table 2. Atomic coordinates and thermal parameters (×10^4 Å^2) at room temperature for $SrC_4H_4O_6{\cdot}4H_2O$ with standard deviations in brackets. The anisotropic thermal parameters are defined as exp[$-2\pi^2(U_{11}a^{*2}h^2 + U_{22}b^{*2}k^2 + U_{33}c^{*2}l^2 + 2U_{23}b^*c^*kl + 2U_{13}a^*c^*hl + 2U_{12}a^*b^*hk)$]. The isotropic thermal parameters (Å^2) for H atoms are listed under U_{11}

Atom	*x*	*y*	*z*	U_{11}	U_{22}	U_{33}	U_{23}	U_{13}	U_{12}
Sr	0.31839(3)	0.19274(3)	0.68474(3)	158(1)	224(1)	184(1)	9(1)	2(1)	3(1)
C(1)	0.1245(3)	0.1625(3)	0.2059(3)	180(11)	231(12)	183(12)	11(9)	1(9)	3(9)
C(2)	0.2821(3)	0.1645(3)	0.2378(3)	143(10)	216(12)	178(11)	-10(9)	23(8)	-5(9)
C(3)	0.3040(3)	0.2254(3)	0.3643(3)	146(11)	196(11)	183(10)	-11(8)	-4(9)	11(9)
C(4)	0.4615(3)	0.2397(3)	0.3976(3)	154(11)	217(12)	216(12)	-4(9)	3(10)	-27(10)
O(1)	0.0605(3)	0.2769(2)	0.2150(2)	206(10)	250(11)	306(12)	-25(8)	-4(9)	35(8)
O(2)	0.0698(3)	0.0481(2)	0.1732(3)	218(10)	239(10)	459(15)	-7(11)	-117(11)	-28(8)
O(3)	0.3401(2)	0.0266(3)	0.2290(2)	186(11)	225(10)	328(12)	-68(9)	36(9)	19(8)
O(4)	0.2340(2)	0.1443(3)	0.4557(2)	150(9)	325(12)	196(9)	14(9)	33(8)	-15(8)
O(5)	0.4894(3)	0.2395(3)	0.5102(2)	179(10)	564(17)	215(11)	23(11)	-36(8)	-86(10)
O(6)	0.5485(2)	0.2573(3)	0.3143(2)	174(9)	393(12)	227(10)	-7(11)	30(9)	-69(9)
O(7)	0.4386(4)	0.4046(4)	0.0572(4)	409(18)	501(20)	521(20)	121(17)	136(17)	7(15)
O(8)	0.5602(5)	0.0749(5)	0.0713(4)	693(26)	505(21)	554(23)	-167(18)	320(20)	-139(21)
O(9)	0.7751(4)	0.3302(4)	0.0787(3)	395(16)	518(21)	258(12)	26(13)	10(11)	98(15)
O(10)	0.8015(4)	0.0373(3)	0.3429(4)	380(18)	297(14)	829(30)	-88(15)	183(19)	-7(13)
H(1)	0.405(6)	0.032(6)	0.183(5)	0.04(2)					
H(2)	0.145(6)	0.187(6)	0.460(5)	0.06(2)					
H(3)	0.328(5)	0.224(5)	0.184(4)	0.02(1)					
H(4)	0.269(6)	0.329(6)	0.367(5)	0.04(2)					
H(5)	0.477(6)	0.428(6)	-0.014(6)	0.07(2)					
H(6)	0.509(6)	0.407(6)	0.117(5)	0.08(2)					
H(7)	0.606(6)	0.148(6)	0.069(5)	0.07(2)					
H(8)	0.587(5)	0.031(5)	0.012(5)	0.06(1)					
H(9)	0.840(6)	0.299(6)	0.044(5)	0.04(2)					
H(10)	0.772(6)	0.406(7)	0.053(6)	0.06(2)					
H(11)	0.732(7)	0.005(7)	0.365(6)	0.07(2)					
H(12)	0.848(6)	-0.017(6)	0.295(6)	0.07(2)					

Table 3. Selected interatomic distances (in Å) and angles (in degrees) for $SrC_4H_4O_6{\cdot}4H_2O$ at room temperature

Sr-O(1)[(a)]	2.559(2)	Sr-O(2)[(b)]	2.527(2)
Sr-O(3)[(b)]	2.616(2)	Sr-O(4)	2.676(2)
Sr-O(5)	2.547(3)	Sr-O(6)[(c)]	2.599(2)
Sr-O(9)[(c)]	2.636(3)	Sr-O(10)[(c)]	2.591(3)
O(1)-C(1)	1.250(4)	O(2)-C(1)	1.257(4)
O(3)-C(2)	1.425(4)	O(4)-C(3)	1.428(4)
O(5)-C(4)	1.263(4)	O(6)-C(4)	1.241(4)
C(1)-C(2)	1.534(4)	C(2)-C(3)	1.518(4)
C(3)-C(4)	1.541(4)		
O(1)-C(1)-O(2)	125.2(3)	O(1)-C(1)-C(2)	116.2(3)
O(2)-C(1)-C(2)	118.5(3)	O(3)-C(2)-C(1)	110.3(2)
O(3)-C(2)-C(3)	111.1(2)	O(4)-C(3)-C(2)	111.9(2)
O(4)-C(3)-C(4)	109.3(2)	O(5)-C(4)-O(6)	125.5(3)
O(5)-C(4)-C(3)	115.7(3)	O(6)-C(4)-C(3)	118.7(3)
C(1)-C(2)-C(3)	110.3(2)	C(2)-C(3)-C(4)	112.5(2)

(Symmetry codes: (a) x+1/2,-y+1/2,-z+1; (b) -x+1/2,-y,z+1/2; (c) x-1/2,-y+1/2,-z+1)

Table 4. Hydrogen bond distances (in Å) and angles (in degrees) for $SrC_4H_4O_6 \cdot 4H_2O$ at room temperature

D-H···A	D-H	H···A	D···A	<D-H···A
O(3)-H(1)···O(8)	0.79(6)	1.96(6)	2.748(4)	172(5)
O(4)-H(2)···O(5)[(a)]	0.94(6)	1.66(6)	2.593(3)	172(5)
C(2)-H(3)···O(7)	0.93(5)	2.45(5)	3.366(5)	173(4)
C(3)-H(4)	1.04(6)			
O(7)-H(5)···O(2)[(b)]	0.89(6)	1.97(6)	2.852(5)	172(6)
O(7)-H(6)···O(3)[(c)]	0.93(6)	2.30(6)	3.212(5)	164(5)
O(8)-H(7)···O(9)	0.81(6)	2.37(6)	3.170(6)	168(5)
O(8)-H(8)···O(10)[(d)]	0.81(5)	2.23(5)	3.022(6)	164(5)
O(9)-H(9)···O(7)[(e)]	0.78(6)	2.42(6)	3.100(6)	147(5)
O(9)-H(10)···O(4)[(f)]	0.78(6)	2.27(7)	3.013(5)	161(6)
O(10)-H(11)···O(7)[(g)]	0.76(6)	2.06(6)	2.822(5)	172(7)
O(10)-H(12)···O(1)[(g)]	0.86(6)	2.14(6)	2.872(4)	142(6)

(Symmetry codes: (a) x-1/2,-y+1/2,-z+1; (b) x+1/2,-y+1/2,-z; (c) -x+1,-y+1/2,-z+1/2; (d) -x+3/2,-y,z-1/2; (e) x+1/2, -y+1/2,-z; (f) -x+1,y+1/2,-z+1/2; (g) -x+1,y-1/2,-z+1/2)

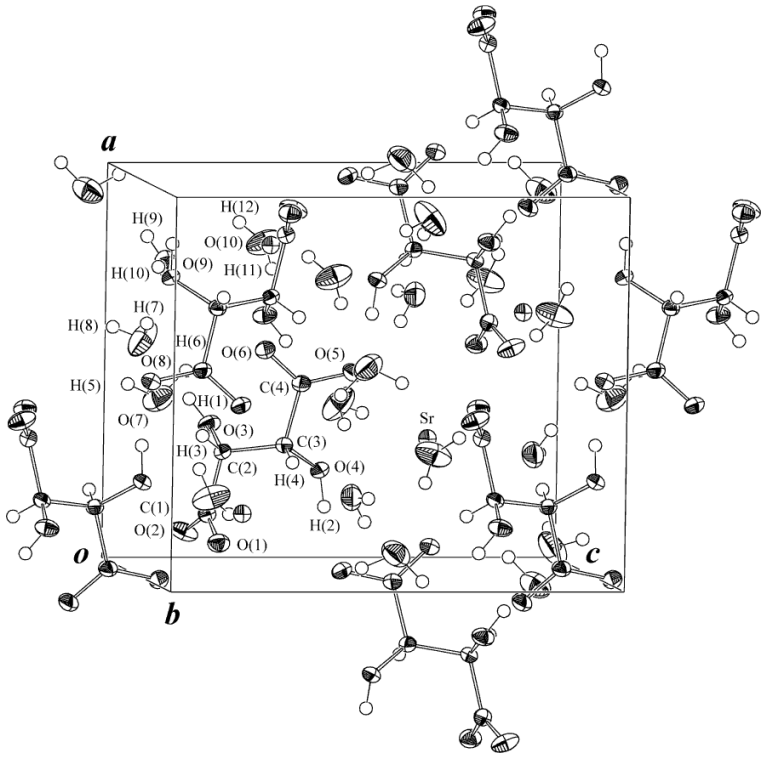

Fig. 1. Perspective view of the $SrC_4H_4O_6 \cdot 4H_2O$ structure at room temperature with 50% probability-displacement thermal ellipsoids

The four H_2O molecules in the structure of $SrC_4H_4O_6 \cdot 4H_2O$ are bonded to $C_4H_4O_6$ molecules or other H_2O molecules. The lengths of the O–H–O hydrogen bonds are in the range of 2.822(5)–3.212(5) Å, as shown in Table 4. There are three different types of hydrogen bond between two neighbouring $C_4H_4O_6$ molecules. One is the O(4)–H(2)–O(5) hydrogen bond, with a bond length of 2.593(3) Å and a bond angle of 172(5)º. The $C_4H_4O_6$ molecules are linked into a chain running along the *a*-axis by this bond. The other hydrogen bonds are the O(7)–H(5)–O(2) and O(7)–H(6)–O(3) bonds formed between the $H_2O(7)$ molecule and two neighbouring $C_4H_4O_6$ molecules. The $H_2O(7)$ molecule is located interstitially between the two neighbouring tartrate molecules. There is a slight difference in the physical and chemical properties of these

hydrogen bonds. The length (2.593(3) Å) of the O(4)–H(2)–O(5) hydrogen bond is shorter than those (2.852(5) and 3.212(5) Å) of the O(7)–H(5)–O(2) and O(7)–H(6)–O(3) bonds formed by the $H_2O(7)$ molecule. Thus, the bonding strength of the O(4)–H(2)–O(5) hydrogen bond between two neighbouring $C_4H_4O_6$ molecules is stronger than those of the hydrogen bonds between $H_2O(7)$ and two neighbouring $C_4H_4O_6$ molecules.

The magnitudes of the thermal parameters for the four oxygen atoms (O(7)–O(10)) in the H_2O molecules are nearly twice those of the O atoms in the $C_4H_4O_6$ molecule, as shown in Table 2. The thermal fluctuations of an atom are considered to be affected by the surrounding atoms and chemical bonds. Therefore, this magnitude difference may be caused by the longer distances between the H_2O molecules and their surrounding atoms (2.748(4)–3.366(5) Å).

3.2 Thermal Analysis

Fig. 2 shows the DSC curve of the $SrC_4H_4O_6{\cdot}4H_2O$ crystal on heating in the temperature range from 105 to 450 K. The weight of the sample (powder) used for the measurement was 3.32 mg, and the heating rate was 5 K min^{-1} under a dry nitrogen flux of 40 ml min^{-1}. Two large endothermic peaks are clearly seen in the DSC curve at 355.7 and 394.2 K, with onset temperatures 337.1 and 392.2 K, respectively. The transition enthalpies ΔH (entropies ΔS) associated with these peaks were determined to be 98.2 (35.0R) and 31.4 kJ mol^{-1} (9.63R), respectively, where R is the gas constant (8.314 $JK^{-1}mol^{-1}$). No significant endothermic or exothermic peaks were observed in the DSC curve between 105 and 337.1 K. Generally, a clear peak in the DSC curve can be attributed to a change of exchange energy at phase transition. Thus, the results indicate that the transitions of $SrC_4H_4O_6{\cdot}4H_2O$ take place at 337.1 and 392.2 K, and there is no phase transition in the temperature range between 105 and 337.1 K. Table 5 shows the peak temperatures, onset temperatures (transition temperatures), transition enthalpies ΔH, and transition entropies ΔS obtained from the DSC curve.

As mentioned above, four non-equivalent water molecules exist in the structure of $SrC_4H_4O_6{\cdot}4H_2O$. The temperatures at which the large peaks are observed in the DSC curve are close to the boiling point of water (373 K). Thus, it is expected that these peaks can be attributed to the evaporation of water molecules. A very small endothermic peak in the DSC curve is also seen at 277.7 K. When the sample used for the above DSC measurement in the temperature range of 105–450 K was remeasured, the small and two large endothermic peaks were not observed in the DSC curve. Thus, the disappearance of the small and large peaks indicates that these peaks are mostly the result of evaporation of water from the sample. In general, there are many defects in the structure of a crystal, such as pores and cracks, and the aqueous solution used for crystal growth can infiltrate the defects. The very small peak at 277.7 K, which is close to 273 K, may be produced by the state change of the solution from ice (solid) to liquid in the defects of the $SrC_4H_4O_6{\cdot}4H_2O$ crystal.

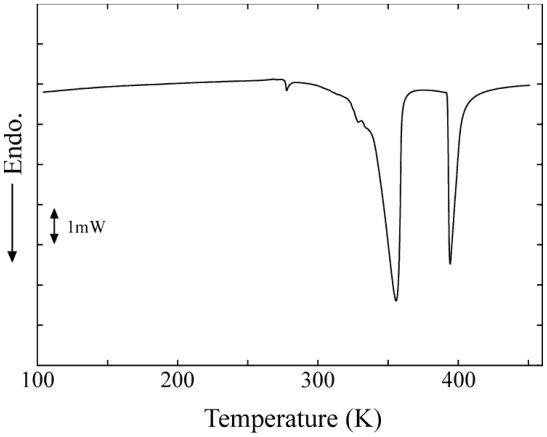

Fig. 2. DSC curve for the $SrC_4H_4O_6{\bullet}4H_2O$ crystal on heating. The sample weight (powder) was 3.32 mg, and the heating rate was 5 K min^{-1} under a dry N_2 flux of 40 ml min^{-1}

Fig. 3 shows the TG, differential TG (DTG), and DTA curves for $SrC_4H_4O_6{\cdot}4H_2O$ in the temperature range of 300–1250 K. The weight of the sample (powder) used for the measurement was 3.46 mg, and the heating rate was 10 K min^{-1} under a dry nitrogen gas flow of 300 ml min^{-1}. The DTA curve exhibits three apparent endothermic peaks at 360.0, 399.3, and 1172.9 K, and three small exothermic peaks at 559.2, 740.1, and 956.7 K. The small peaks are indicated by arrows in Fig. 3. An enlarged view of the curve around 550 K is also shown (Fig. 3, inset). In this enlarged view, a very small endothermic peak can be observed on the curve at 546.1 K, which is close to the exothermic peak

at 559.2 K. The observed DTA peaks at 360.0 and 399.3 K correspond to the above-mentioned DSC peaks at 355.7 and 394.2 K, respectively. The slight differences of about 5 K between the peak temperatures are probably caused by the different heating rates (5 or 10 K min^{-1}) and sample pans (aluminium or alumina) used for these measurements. The obtained TG and DTA curves are very different from those reported previously for $SrC_4H_4O_6{\cdot}4H_2O$ and $CaC_4H_4O_6{\cdot}4H_2O$, except for the DTA curve below 473 K for calcium tartrate [21-23]. The DTA curve of calcium tartrate clearly showed two endothermic peaks at 384.3 and 437.4 K, which may correspond to the peaks observed at 360.0 and 399.3 K, respectively, in the DTA curve in this study.

Table 5. Peak temperatures, onset temperatures (transition temperatures), transition enthalpies *ΔH*, and transition entropies *ΔS* for $SrC_4H_4O_6{\cdot}4H_2O$ obtained from DSC, DTA, and DTG curves

DSC	Peak temp. (K)	355.7	394.2					
	Onset temp. (K)	337.1	392.2					
	ΔH (kJ mol^{-1})	98.2	31.4					
	ΔS/*R*	35.0	9.63					
DTA	Peak temp. (K)	360.0	399.3	546.1	559.2	740.1	956.7	1172.9
	Onset temp. (K)	343.6	393.7	537.1	552.7	729.3	943.0	—
DTG	Peak temp. (K)	358.3	395.9	—	564.3	741.9	956.6	1169.1

(Gas constant R = 8.314 $JK^{-1}mol^{-1}$)

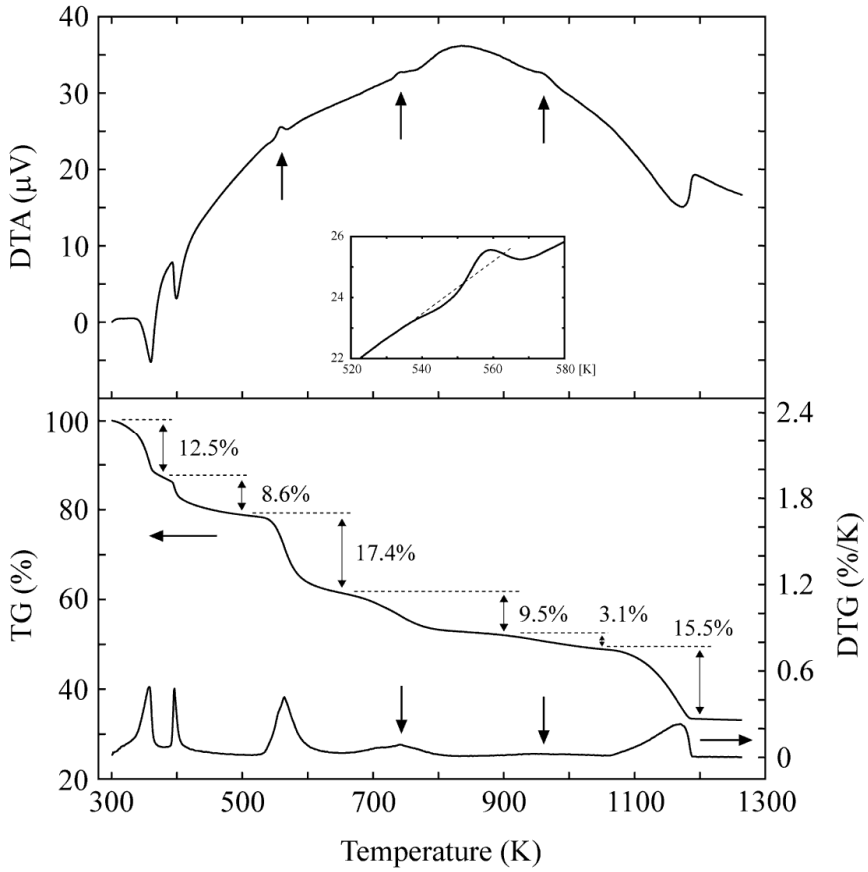

Fig. 3. TG, DTG, and DTA thermograms for the $SrC_4H_4O_6{\cdot}4H_2O$ crystal on heating. The inset figure shows an enlarged view of the curve around 550 K. The sample weight (powder) was 3.46 mg, and the heating rate was 10 K min^{-1} under a dry N_2 flux of 300 ml min^{-1}

The DTG curve in Fig. 3 has peaks at 358.3, 395.9, 564.3, 741.9, 956.6, and 1169.1 K. The peak temperature of 956.6 K was determined from the numerical data for the DTG curve, as no obvious peak was detected around the temperature in the curve. These DTG peaks correspond to the respective DTA peaks. As the DTG curve is the first derivative of the TG curve, the DTA peaks are associated with the rate of weight loss on the TG curve. Table 5 also shows the peak temperatures and onset temperatures (transition temperatures) obtained from the DTA and DTG curves.

The TG curve shows the temperature dependence of the weight loss of the $SrC_4H_4O_6{\cdot}4H_2O$ crystal. The weight loss around 360.0 K in the TG curve (determined over the temperature range from 300 to 375 K) was 12.5%, and that around 399.3 K (determined over the temperature range from 375 to 500 K) was 8.6%. As mentioned above, it is expected that the two endothermic peaks around 373 K are caused by the evaporation of bound water molecules. The theoretical weight loss caused by the elimination of two H_2O molecules from the $SrC_4H_4O_6{\cdot}4H_2O$ crystal is calculated to be 11.7% [=2×18.02/307.75], whereas that caused by the elimination of one H_2O molecule is calculated to be 5.9% [=18.02/307.75]. These values are close to the experimental weight losses of 12.5% and 8.6% around 360.0 and 399.3 K, respectively. The different evaporation temperatures are probably caused by differences in the hydrogen bonding strength between the H_2O molecule and its surrounding ions, as mentioned in section 3.1, and thus, by differences in the O–H–O hydrogen bond length. The lengths of the hydrogen bonds originating from the H_2O molecules are in the range of 2.822(5)–3.212(5) Å. The slightly shorter bond lengths of 2.852(5) and 2.822(5) Å are observed for $H_2O(7)$ and $H_2O(10)$ molecules, respectively. Thus, the weight loss around 360.0 K is considered to be caused by the evaporation of $H_2O(8)$ and $H_2O(9)$ molecules.

Very small endothermic and exothermic peaks were observed at 546.1 and 559.2 K in the DTA curve, respectively. It is believed that endothermic and exothermic peaks in a DTA curve, accompanied by decomposition at high temperature, are due to evaporation and the formation of products, respectively. Thus, these two processes are considered to have taken place around 550 K. We assume that the weight loss is caused by the elimination of the remaining H_2O molecule and H_2CO gas formed from $2H^+$ and CO^{2-} ions. The theoretical weight loss is calculated to be 15.6% [=(18.02+30.03)/307.75]. This value is very close to the experimental weight loss of 17.4% around 550 K determined from the TG curve over the temperature range from 500 to 650 K. Because small exothermic peaks at 740.1 and 956.7 K were observed in the DTA curve, the formation of products, which we assume are H_2CO and $1/2O_2$, respectively, also occurs at these temperatures. The theoretical weight losses caused by the eliminations of H_2CO and $1/2O_2$ gases are calculated to be 9.8% [=30.03/307.75] and 5.2% [=16.00/307.75], respectively. These values are close to the respective experimental weight losses of 9.5% and 3.1% around 740.1 and 956.7 K determined from the TG curve over the temperature ranges of 650–900 K and 900–1050 K, respectively. An endothermic peak was observed at 1172.9 K in the DTA curve, indicating that an evaporation reaction due to thermal decomposition occurs around this temperature. The theoretical weight loss caused by the evolution of 2CO gas is calculated to be 18.2% [=2×28.01/307.75]. This value is close to the experimental weight loss of 15.5% around 1172.9 K determined from the TG curve over the temperature range of 1050–1200 K. The experimental and theoretical weight losses, the molecules eliminated by evaporation, and the evolved gases at the various temperature ranges are summarized in Table 6.

Finally, the total theoretical weight loss from $SrC_4H_4O_6{\cdot}4H_2O$ is calculated to be 66.3%. This

Table 6. TG results for the $SrC_4H_4O_6{\cdot}4H_2O$ decomposition process

Temp. range [K]	Weight loss (obs.) [%]	Weight loss (cal.) [%]	Elimination molecules
300–375	12.5	11.7	$2H_2O$
375–500	8.6	5.9	H_2O
500–650	17.4	15.6	H_2O + H_2CO gas
650–900	9.5	9.8	H_2CO gas
900–1050	3.1	5.2	$1/2O_2$ gas
1050–1200	15.5	18.2	2CO gas
Total	66.6	66.3	

value is very close to the total experimental weight loss of 66.0%. Thus, the slight differences between the experimental and theoretical weight loss values are probably caused by overlapping of the temperature ranges corresponding to the decomposition reactions. After the measurement, a chalky white substance remained in the open vessel. The white substance is suggested to be strontium oxide (SrO), the formation of which is described below.

Summarizing the considerations mentioned above, the chemical reactions involved in the thermal decomposition of $SrC_4H_4O_6{\cdot}4H_2O$ can be described by the following chemical equations:

$$SrC_4H_4O_6{\cdot}4H_2O \rightarrow SrC_4H_4O_6{\cdot}2H_2O + 2H_2O$$
$$SrC_4H_4O_6{\cdot}2H_2O \rightarrow SrC_4H_4O_6{\cdot}H_2O + H_2O$$
$$SrC_4H_4O_6{\cdot}H_2O \rightarrow SrC_3H_2O_5 + H_2CO + H_2O$$
$$SrC_3H_2O_5 \rightarrow SrC_2O_4 + H_2CO$$
$$SrC_2O_4 \rightarrow SrC_2O_3 + 1/2O_2$$
$$SrC_2O_3 \rightarrow SrO + 2CO.$$

4. CONCLUSION

Single crystals of strontium tartrate tetrahydrate, $SrC_4H_4O_6{\cdot}4H_2O$, were grown in silica gel medium at 308 K by a diffusion method. The thermal properties and crystal structure of the single crystals were studied by DSC, TG-DTA, and X-ray diffraction measurements. The crystal structure at room temperature was determined to be orthorhombic with space group $P2_12_12_1$ by means of single-crystal X-ray diffraction. It was confirmed that the structure consists of SrO_8 dodecahedra and a hydrogen-bonding network along the *a*-axis between adjacent $C_4H_4O_6$ molecules, which is very similar to the structure of $CaC_4H_4O_6{\cdot}4H_2O$ reported in previous papers. Weight losses during the thermal decomposition of $SrC_4H_4O_6{\cdot}4H_2O$ occurred in the temperature range of 350–1200 K. The chemical equations illustrating the decomposition reactions of $SrC_4H_4O_6{\cdot}4H_2O$ were presented with the corresponding temperature ranges. It was suggested that the weight losses were caused by the evaporation of bound H_2O molecules and the evolution of H_2CO, $1/2O_2$, and 2CO gases, and the resulting chalky white substance in the open vessel after decomposition was strontium oxide.

COMPETING INTERESTS

Authors have declared that no competing interests exist.

REFERENCES

1. Buschmann J, Luger P. Structure of potassium hydrogen (+)-tartrate at 100 K, $K^+.C_4H_5O_6^-$. Acta Crystallogr. 1985;C41(2): 206-208.
   Available:http://dx.doi.org/10.1107/S0108270185003341
2. Desai CC, Patel AH. Crystal data for ferroelectric $RbHC_4H_4O_6$ and $NH_4HC_4H_4O_6$ crystals. J Mater Sci Lett. 1988;7(4):371-373.
   Available:http://link.springer.com/article/10.1007/BF01730747
3. Labutina ML, Marychev MO, Portnov VN, Somov NV, Chuprunov EV. Second-order nonlinear susceptibilities of the crystals of some metal tartrates. Crystallogr. Reports. 2011;56(1):72-74.
   Available:http://dx.doi.org/10.1134/S1063774510061082
4. Silgo CG, Platas JG, Pérez CR, López T, Torres M. Barium L-tartrate. Acta Crystallogr. 1999;C55(5):740-742.
   Available:http://dx.doi.org/10.1107/S0108270198016709
5. De Ridder DJA, Goubitz K, Sonneveld EJ, Molleman W, Schenk H. Lead tartrate from X-ray powder diffraction data. Acta Crystallogr. 2002;C58(12):m596-m598.
   Available:http://dx.doi.org/10.1107/S0108270102019637
6. Weil M. Crystal structure of lead(II) tartrate: A redetermination. Acta Crystallogr. 2015;E71(1):82-84.
   Available:http://dx.doi.org/10.1107/S2056989014027376
7. Hawthorne FC, Borys I, Ferguson RB. Structure of calcium tartrate tetrahydrate. Acta Crystallogr. 1982;B38(9):2461-2463.
   Available:http://dx.doi.org/10.1107/S0567740882009042
8. Boese R, Heinemann O. Crystal structure of calcium tartrate tetrahydrate, $C_4H_4O_6Ca(H_2O)_4$. Z. Kristallogr. 1993; 205(1-2):348-349.
   Available:http://dx.doi.org/10.1524/zkri.1993.205.12.348
9. Bohandy J, Murphy JC. An X-ray study of gel-grown strontium tartrate tetrahydrate. Acta Crystallogr. 1968;B24(2):286-287.
   Available:http://dx.doi.org/10.1107/S0567740868002141
10. Ambady GK. The crystal and molecular structures of strontium tartrate trihydrate and calcium tartrate tetrahydrate. Acta Crystallogr. 1968;B24(11):1548-1557.

Available:http://dx.doi.org/10.1107/S0567740868004619
11. Vijayakumari T, Padma CM, Mahadevan CK. Effect of Co doping on the structural and physical properties of $SrC_4H_4O_6.3H_2O$ and $SrC_4H_4O_6.4H_2O$ crystals. Int J Mod Eng Res. 2014;4(12):1-9.
Available:http://www.ijmer.com/papers/Vol4_Issue12/Version-3/A0412_03-0109.pdf
12. Abdel-Kader MM, El-Kabbany F, Taha S, Abosehly AM, Tahoon KK, El-Sharkawy AA. Thermal and electrical properties of ammonium tartrate. J Phys Chem Solids. 1991;52(5):655-658.
Available:http://www.sciencedirect.com/science/journal/00223697/52/5
13. Torres ME, Peraza J, Yanes AC, López T, Stockel J, López DM, Solans X, Bocanegra E, Silgo GG. Electrical conductivity of doped and undoped calcium tartrate. J Phys Chem Solids. 2002;63(4):695-698.
Available:http://www.sciencedirect.com/science/journal/00223697/63/4
14. Firdous A, Quasim I, Ahmad MM, Kotru PN. Dielectric and thermal studies on gel grown strontium tartrate pentahydrate crystals. Mull Mater Sci. 2010;33(4):377-382.
Available:http://dx.doi.org/10.1007/s12034-010-0057-1
15. Pasteur ML. Sur les relations qui peuvent existre la forme cristalline, la composition chimique et Le sens de la polarisation rotatoire. Ann Chim Phys. 1848;24:442-463.
Available:http://gallica.bnf.fr/ark:/12148/bpt6k65691733/f446.image.r=Annales%20de%20chimie%20et%20de%20physique.langEN
16. Gal J. Citation for chemical breakthrough awards: Choosing pasteur's award-winning publication. Bull Hist Chem. 2013;38(1):7-12.
Available:http://www.scs.illinois.edu/~mainzv/HIST/awards/Citations/v38-1%20p7-12.pdf
17. Tobe Y. The reexamination of Pasteur's experiment in Japan. Mendeleev Commun. 2003;13(3):93-94.
Available:http://dx.doi.org/10.1070/MC2003v013n03ABEH001803
18. Burla MC, Caliandro R, Camalli M, Carrozzini B, Cascarano GL, Giacovazzo C, Mallamo M, Mazzone A, Polidori G, Spagna R. SIR2011: A new package for crystal structure determination and refinement. J Appl Crystallogr. 2012;45(2):357-361.
Available:http://dx.doi.org/10.1107/S0021889812001124
19. Sheldrick GM. Crystal structure refinement with SHELXL. Acta Crystallogr. 2015;C71(1):3-8.
Available:http://dx.doi.org/10.1107/S2053229614024218
20. Farrugia LJ. WinGX and ORTEP for Windows: An update. J Appl Crystallogr. 2012;45(4):849-854.
Available:http://dx.doi.org/10.1107/S0021889812029111
21. Rahimkutty MH, Babu KR, Pillai KS, Kumar MRS, Nair CMK. Thermal behaviour of strontium tartrate single crystals grown in gel. Bull Mater Sci. 2001;24(2):249-252.
Available:http://dx.doi.org/10.1007/BF02710110
22. Shajan XS, Mahadevan C. On the growth of calcium tartrate tetrahydrate single crystals. Bull Mater Sci. 2004;27(4):327-331.
Available:http://dx.doi.org/10.1007/BF02704767
23. Pradyumnan PP, Shini C. Growth characterization and etching studies of calcium tartrate single crystal grown using tamarind extract. Indian J Pure Appl Phys. 2009;47(3):199-205.
Available:http://nopr.niscair.res.in/bitstream/123456789/3443/1/IJPAP%2047(3)%20199-205.pdf

Peer-review history:
The peer review history for this paper can be accessed here:
http://sciencedomain.org/review-history/13060